Calibration of Historical and Future AVHRR and GOES Visible and Near-Infrared Sensors and the Development of a Consistent Long-Term Cloud and Clear-Sky Radiation Property Dataset

Project Report
12/1/2010 – 12/31/2013
Award: NA10AANEG0158

Principal Investigator: Patrick Minnis (p.minnis@nasa.gov)
NASA Langley Research Center, Hampton, VA

Co-Investigators: David R. Doelling, Kristopher M. Bedka
NASA Langley Research Center, Hampton, VA

Xiangqin Wu
NOAA NESDIS, Silver Spring, MD

Xiaxiong Xiong
NASA Goddard Space Flight Center

CDRs Addressed

Multispectral Imager(s) Solar Reflective (FCDR)
Cloud Properties (Amount, Height, Phase, Optical Depth, Effective Particle Size) TCDR
Clear-Sky Skin Temperature TCDR

1. Introduction

A stable and consistent set of imager radiances is an essential component of any long-term satellite climate data record (CDR). Calibrated imager radiances are critical for retrieving climate quality geophysical parameters needed for monitoring climate. Two sets of those parameters, cloud properties and the properties of the complementary clear scenes, are important components of the climate system since they affect the radiation balance and hydrological cycle. While several different groups around the world are involved in calibrating imagers on polar orbiters such as the Advanced Very-high Resolution Radiometer (AVHRR) series, and on geostationary satellite (GEOsat) imagers, there are many different methods for effecting those calibrations. Similarly, cloud and surface climatologies are being or have been developed by different groups around the globe, but the satellite imager data are being analyzed in different ways resulting in differences among the results. It is this variety of methods and results that helps establish the uncertainties in the resulting calibrations and geophysical parameters allowing an assessment of the confidence in their climatological variations. This project focuses on two goals, imager solar channel calibration to develop a coherent reflected radiance Fundamental CDR (FCDR) and cloud and clear-sky property retrievals to provide a Thematic CDR (TCDR) of cloud and clear parameters consistent with their counterparts determined for the Clouds and Earth's Radiant Energy System (CERES). CERES is a climate project charged with monitoring the Earth's radiation budget, the fundamental energy source driving weather and climate. This report summarizes the work accomplished during the period, December 2010 – December 2013.

1.1 Calibration FCDR

The calibration FCDR is focused on the development of a coherent reflected radiance Fundamental CDR (FCDR) for the AVHRR and geostationary satellite (GEOsat) imagers extending back to 1978. To accomplish this goal, we are applying mature and robust calibration algorithms, specifically, the Nearly Simultaneous Ray-matched Technique (NSRT), stable desert target method (SDTM), and the Deep Convective Cloud Technique (DCCT). These methods were used to uncover errors in the MODIS and TRMM VIRS records for visible and infrared calibrations. We are developing a semi-automated method for applying the methods and applying them in real time with quality control constraints. Uncertainties will be developed from comparisons of results from the three methods.

1.2 Cloud and clear TCDR

The cloud TCDR consists of cloud fraction CF , phase, optical depth (COD), effective particle size CER, height, and temperature. The clear TCDR will consist of clear-sky albedos and clear-sky surface skin effective temperatures. These TCDR parameters are being developed in a manner that is as consistent as possible with that used to retrieve the CERES cloud properties from the MODerate-resolution Imaging Spectroradiometer (MODIS). To date, the CERES cloud properties have been derived using MODIS data since 2000 and will continue to be retrieved using data from the Visible Infrared Imager Radiometer Suite (VIIRS) on future low Earth-orbiting satellites (LEOsats). Because the CERES Edition-4 analysis uses more than seven of the MODIS channels (Minnis et al., 2010a), modifications have been made to the algorithms for application to the 5-channel AVHRR data. The results of this analysis should be extremely valuable for climate studies.

2. Accomplishments to date

2.1 AVHRR Calibration FCDR

The FCDR imager calibration portion of this project at NASA Langley Research Center (LaRC) was begun with the goal of providing data from different satellites that could be used to retrieve consistent cloud and surface properties across platforms and decades with short term predictive capability for currently operating satellites, which can provide near-real time data for nowcasting and other weather applications, such as model assimilation. The approach is to normalize each relevant imager channel to a corresponding channel on the Aqua MODIS. The choice of Aqua MODIS is based on its stability, relatively small degradation, and onboard calibration systems for solar and infrared channels. To effect the transfer of the MODIS calibrations to other satellites, it is necessary to 1) account for the spectral response function (SRF) differences between a given imager channel and its MODIS counterpart, 2) transfer the calibrations back and forward in time by inter-satellite crossovers and a variety of other vicarious techniques, and 3) account for eccentricities in a given channel's behavior. The effort is being conducted independently and in collaboration with the Global Space-based Inter-Calibration System (GSICS, Goldberg et al., 2011). (D. Doelling is a leading member of the GSICS solar channel calibration research working group). We are funded to intercalibrate the visible (VIS; ~0.65 μm), vegetation (VEG; ~0.87 μm), and near-infrared (NIR; ~1.6 μm) channels on all AVHRRs. We planned to rely on calibrations of the AVHRR shortwave infrared (SIR; ~3.7 – 4.0 μm), infrared window (IRW; ~11 μm), and split window (SWC; ~12 μm) channels by other SDS team members, but that information has not been available. Therefore, we have performed some infrared channel calibration studies.

2.1.1 Reference channels

The Aqua MODIS channels were examined to assess the uncertainties in these references (Minnis et al. 2008, Wu et al. 2013) and, to extend the utility of the Aqua MODIS channel, it was first used to calibrate the Terra MODIS channels (Doelling et al. 2014). The SRFs for each AVHRR channel are normalized to the MODIS reference using spectral band adjustment factors (SBAFs) derived for solar channels by integrating high-resolution (1-nm) spectral radiances measured by the ENVISAT SCanning Imaging Absorption spectroMeter for Atmospheric CartograpHY (SCIAMACHY) over each SRF to determine the relationship between the MODIS and target channels (Doelling et al. 2012, 2013a). The necessity for using the SBAFs was shown in detail by Chander et al. (2013). Scarino et al. (2013) demonstrated that the SCHIAMACHY pseudo-VIS and the Aqua MODIS VIS radiances agree to within 1.5%, which is within the 2% uncertainty in the MODIS absolute calibration. These results show that the data can be used interchangeably to that level of uncertainty. SBAFs are scene dependent and therefore must be used carefully.

2.1.2 Ray-matching (RM) method

The transfer of the solar channel calibrations during the MODIS era is accomplished using several different approaches. The most direct method is by ray matching (RM). In this approach, the reference and target imager must view the same area within specified time and viewing angle windows. Typically, the average radiances from both satellites meeting the RM criteria are computed for a specified area (e.g., 0.5° region) over the course of a month with the reference radiances adjusted to time and SRF of the target channel using the ratio of the cosines of the solar zenith angle (SZA) and the SBAFs, respectively. The RM is one of the techniques being used for GSICS (Doelling et al. 2011a).

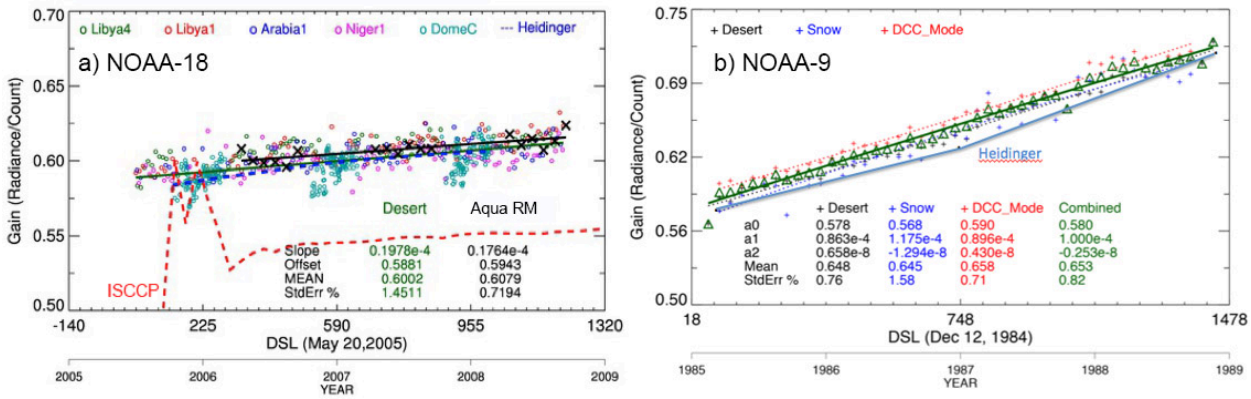

Fig. 1. Gains for AVHRR channel 1 (VIS) using various techniques.

2.1.3 Deep convective cloud (DCC) and stable surface target techniques

Another method used for GSICS is the Deep Convective Cloud (DCC) technique (Doelling et al. 2011b), which assumes that the DCC reflectance means or modes for a given area and period are invariant over time (Doelling et al. 2013b). The DCC method requires use of the same target areas for a given satellite and variations in the bidirectional distribution function (BRDF) with viewing angels and albedo with SZA must be taken into account.

Vicarious calibration using stable desert targets is a long-used technique for calibrating satellites. It is utilized in this project also, but with some significant refinements. A daily exoatmospheric radiance model (DERM) was constructed for each desert site using a well-calibrated (via RM) GEOsat to fully characterize the variation of reflectance with uncertainties over the course of the day for all seasons (Bhatt et al. 2012, 2013a). Assuming the desert albedos do not vary at decadal scales, these sites can be used to calibrate historical GEOsats and LEOsats with pertinent BRDF corrections. Additionally, high altitude polar sites, Greenland and Dome-C, Antarctica, are also used as stable bright targets for additional LEOsat calibration.

2.1.4 Best estimate determination

Uncertainties and errors in the intercalibrations are estimated by comparing the results from the different techniques and by applying reference-based RM calibrations from one target to a second target by either RM or one of the other methods and comparing the retrieved gains with that derived from the reference-based RM calibration for the second target. While RM comparisons based on the reference data are assumed to be the most accurate technique, a combination of the methods is used to determine a best estimate of the time-dependent gain for a given channel on historical imagers. This approach averages the gains from each approach weighted by the variance of the data about the trend line for each method.

Figure 1 shows results from the various methods for the NOAA-18 (Fig. 1a) and NOAA-9 (Fig. 1b) AVHRR VIS channels. Also included are the results from the International Satellite Cloud Climatology Project (ISCCP, Rossow and Schiffer 1999) and from Heidinger et al. (2010). Figure 1a includes the RM, desert, and Dome C site results. The fixed site results include every overpass used, while the RM results are from monthly datasets. These show that fixed site results and the RM gains differ by less than 1%, while the desert values are quite close to the Heidinger et al. (2010) results. The NOAA-9 gains lack the RM results since the MODIS data were not available in the 1980's. The DCC results are included, however, and when combined with the surface yield the best estimate (green curve), which differs by less than 1% from any of the other techniques. The gains from Heidinger et al. (2010) are 1 – 2.5% less than those from

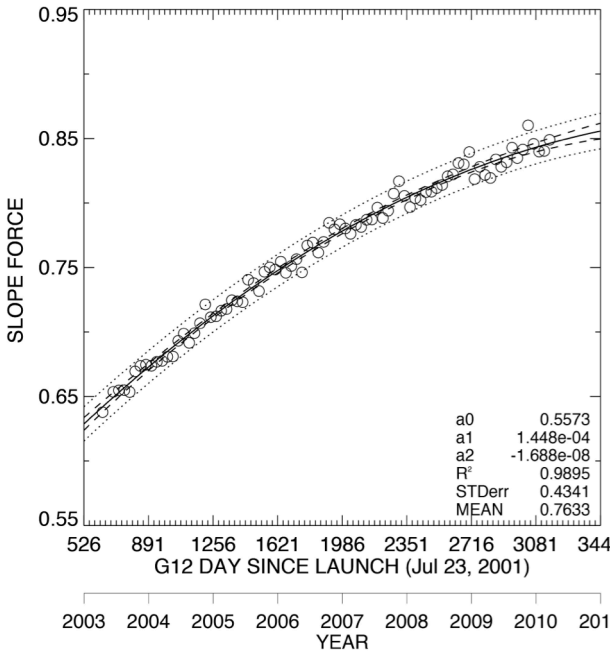

Fig. 2. GOES-12 VIS channel gain derived using RM method with Aqua channel 1.

the LaRC methods. To date, gains for VIS, VEG, and NIR channels available on AVHRR have been normalized to MODIS for NOAA-9 through NOAA-19 and MetOp-A. Gains for all GOES solar channels since 2000 have been normalized to the corresponding MODIS channels. Figure 2 shows the variation of the GOES-12 VIS channel as a function of time since launch. It includes the quadratic regression fit and the uncertainty bounds.

2.1.5 Infrared channel calibrations

In testing the cloud mask for various AVHRRs, some difficulties were encountered that arose from calibration and other characteristics of some IR channels. While those calibrations were expected from other components of the SDS system to provide stable, consistent IR calibrations, such information has not become available. Thus, we have relied on our own adjustments for some anomalies and mis-calibrations. For example, the RM method can be used to transfer the Aqua and Terra MODIS calibrations (after adjustment using IASI data) to contemporaneous GOES and AVHRRs.

Finally, in the process of performing the various calibration exercises, certain instrument artifacts were detected that require correction whenever possible. One of these is the low-end correction of the SIR channels at night. This was noticed when comparing Terra and Aqua MODIS (Minnis et al. 2008) RM data at night. LaRC corrected it for Terra MODIS by fitting an error function to the data at temperatures less than ~ 250K. Figure 3 shows the nonlinear nighttime behavior of the SIR channels on the NOAA-18 and NOAA-15 AVHRRs relative to the closest Aqua MODIS SIR channel. To date, no corrections have been made for this and other artifacts that might affect the IR channels.

2.1.6 Deliveries

The calibration component of this project has been documented in the FCDR CATBD (Doelling and Minnis, 2013). Also, the FCDR Implementation plan has been delivered and approved at NCDC.

2.2 AVHRR cloud and clear properties TCDR

An automated analysis system has been set up that reads in all of the appropriate inputs and processes a month of AVHRR cloud data. The refined algorithms are undergoing final testing. AVHRR GAC level 1B format data acquired from the NOAA CLASS system comprise the primary radiance dataset used here. The LaRC algorithms and scripts are referred to as the AVHRR Modular Cloud Property Retrieval System (AMCPRS). The AMCPRS processes pixel data at the tile level; each tile has a dimension of 12 scan lines by 8 pixel elements to approximate the CERES cloud processing system (Minnis et al. 2011a).

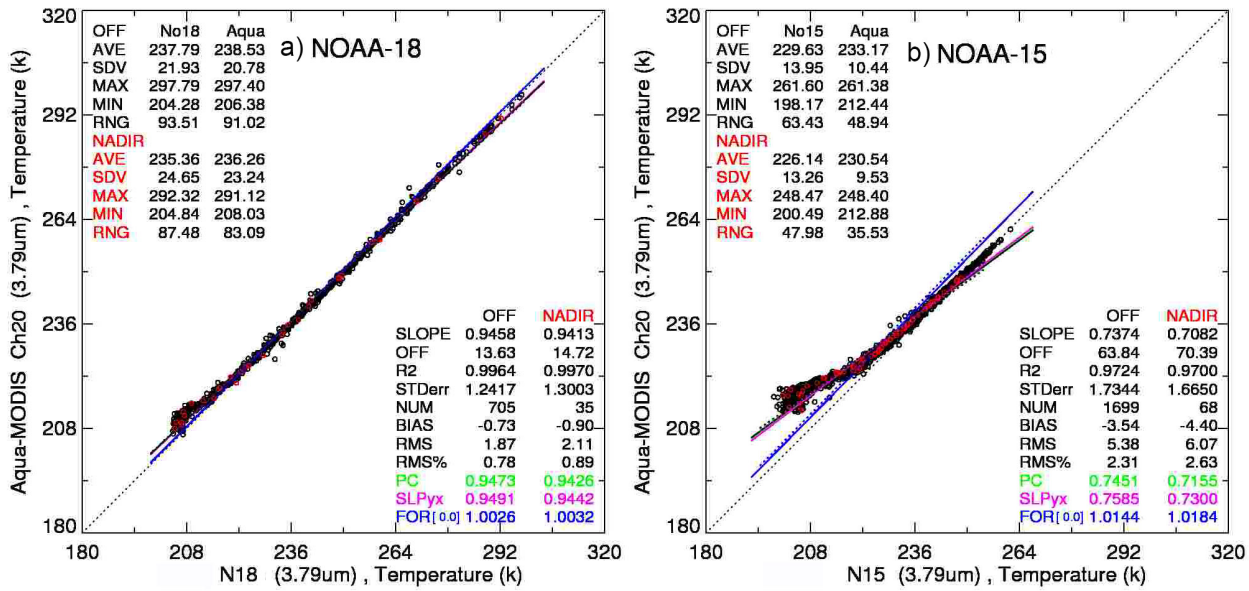

Fig. 3. RM data regression for Aqua MODIS matched to (a) June 2006 NOAA-18 and (b) June 2003 NOAA-15 SIR data at night.

2.2.1 Data preprocessing: re-navigation and filtering

In addition to calibration, Simpson and Yhann (1994) and references therein together with our practical experience reveal that the original Level 1B data exhibit a number of issues that render the data unsuitable for direct input into TCDR processing. These problems include:

1) Random bad scan lines throughout an orbit

2) Navigation errors up to 200 km in magnitude

3) Periodic striping in pre-NOAA-15 SIR data

4) Noise at very cold SIR BTs, most notably in pre-NOAA-15 data

5) Noise at very warm SWC BTs, noted in NOAA-9 data but possibly present in other satellites.

An AVHRR pre-processing software package (referred to as SAPS) has been developed to address these issues to the fullest possible extent. This software ingests a GAC Level 1B file, correctly navigates and noise filters the data, and writes out a NetCDF-4 file that includes all parameters needed by AMCPRS. SAPS processes a typical GAC file in approximately 75 seconds. The navigation correction component of this software is described in detail by Khlopenkov et al. (2010). An example of this navigation correction is shown in Fig. 4 (top).

Periodic noise (striping) in the SIR brightness temperatures (BT) is diminished by applying a fast Fourier Transform analysis. At the low end of it dynamic range, the AVHRR SIR channel is plagued by increasing random noise with decreasing temperatures. To address this problem, the lower end of the count-temperature lookup table (LUT) is extended to give values to occasional counts beyond the range of the provided LUT. After this is applied, spatial smoothing is used to reduce the noise. The smoothing is based on a 2-dimensional cubic convolution algorithm with a Gaussian kernel. The Gaussian profile defines the weights for the neighboring pixels: the further

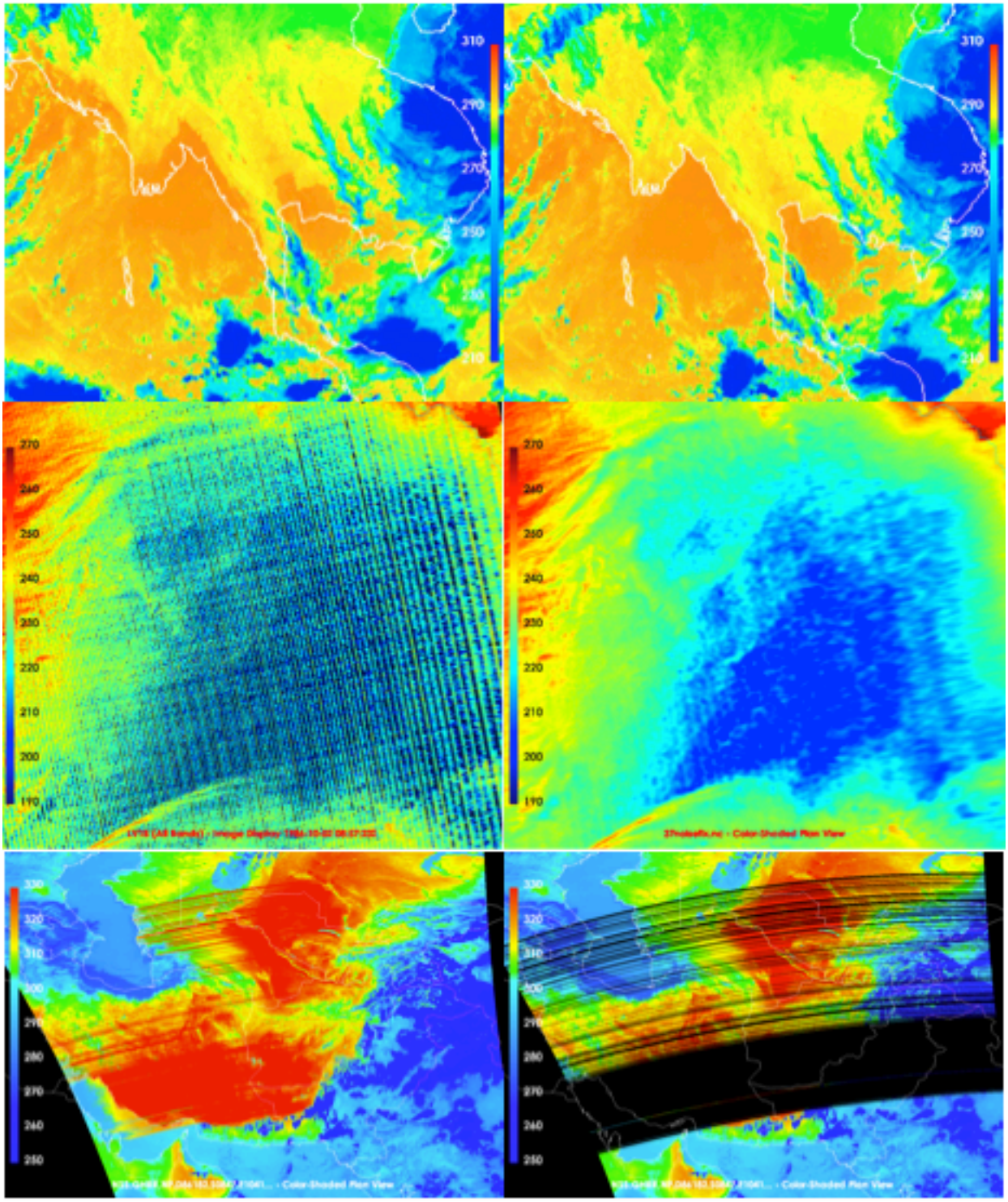

Fig. 4. Examples of AVHRR Level 1B data problems addressed by AVHRR SAP pre-processing software. (top) Color-enhanced NOAA-18 10.8-µm BT image over southeast Asia before (left) and after (right) navigation correction. The BT gradient in this scene associated with land/ocean temperature differences should align with the coastline (white line). (middle) Color-enhanced NOAA-9 3.7-µm imager over Antarctica before (left) and after (right) noise filtering. (top) Color-enhanced NOAA-9 12.0-µm image over Central Asia before (left) and after (right) noise filtering.

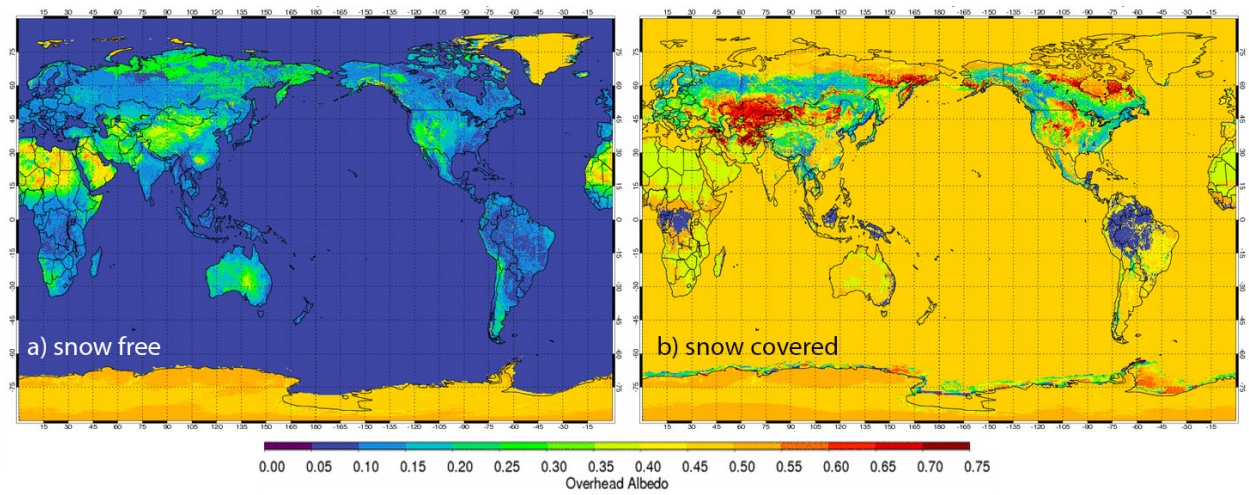

Fig. 5. Clear-sky VIS overhead-sun albedos for January.

from the current pixel, the lower the weight. Thus, the characteristic sigma of the kernel determines the smoothing strength. An example of this filtering is shown in Fig. 4 (middle).

To account for corrupt data across several scan lines and isolated noise, a special algorithm was developed to detect and discard corrupt scan lines and noisy pixels. The algorithm uses 3 metrics to determine if a scan line contains noise: (1) sum of square differences (SSD) between neighboring pixels within one scan line; (2) SSD of pixel pairs between neighboring lines, and (3) SSD between pixels in the same line of the IRW and SWI images. Each of these metrics is required to change gradually from line to line as it should in uncorrupted data. Figure 4 (bottom) shows the result of this noise filtering where scan lines with bad data are replaced with missing values (black). Minnis and Bedka (2014) describe these preprocessing methods in detail.

2.2.2 Clear-sky radiance estimation

To detect clouds, it is necessary to know the radiance characteristics of the viewed scene when it is cloud free. In the AMCPRS, the clear-sky radiances are estimated for a given tile using the NASA's Modern-Era Retrospective Analysis for Research and Applications (MERRA, Rienecker et al. 2011) surface skin temperatures and the surface emissivities used by CERES (Minnis et al. 2008) to predicted the IRW, SIR, and SWC BTs leaving the surface. A set of correlated *k*-distribution absorption coefficients were developed for each channel to calculate the absorption and emission of the atmosphere using the MERRA profiles. The results are used with the surface-leaving BTs to estimate the clear-sky BTs that would be measured by each AVHRR IR channel.

For the VIS channel, the clear-sky reflectances over land and snow-covered surfaces are estimated from overhead-sun clear-sky albedo maps at a 10’ resolution. The albedos are first corrected for their SZA dependence and then a normalized bidirectional distribution function (BRDF) is applied to estimate the clear-sky reflectance at the specified viewing angles. The clear-sky reflectance over ocean is estimated as a function of wind speed using a theoretical model. The initial clear-sky albedo maps were constructed using the clear-sky MODIS results of Minnis et al. (2011b) for each month. These maps were then used to analyze a year of NOAA-18 AVHRR data from which the clear-sky results were extracted to produce a new set of initial AMCPRS clear-sky albedo maps for each month of the year. Those maps serve as input for the cloud mask and analysis and are updated as the data are processed. The result is a new starting map for each month in sequence. The analysis of the cloud properties uses the updated maps

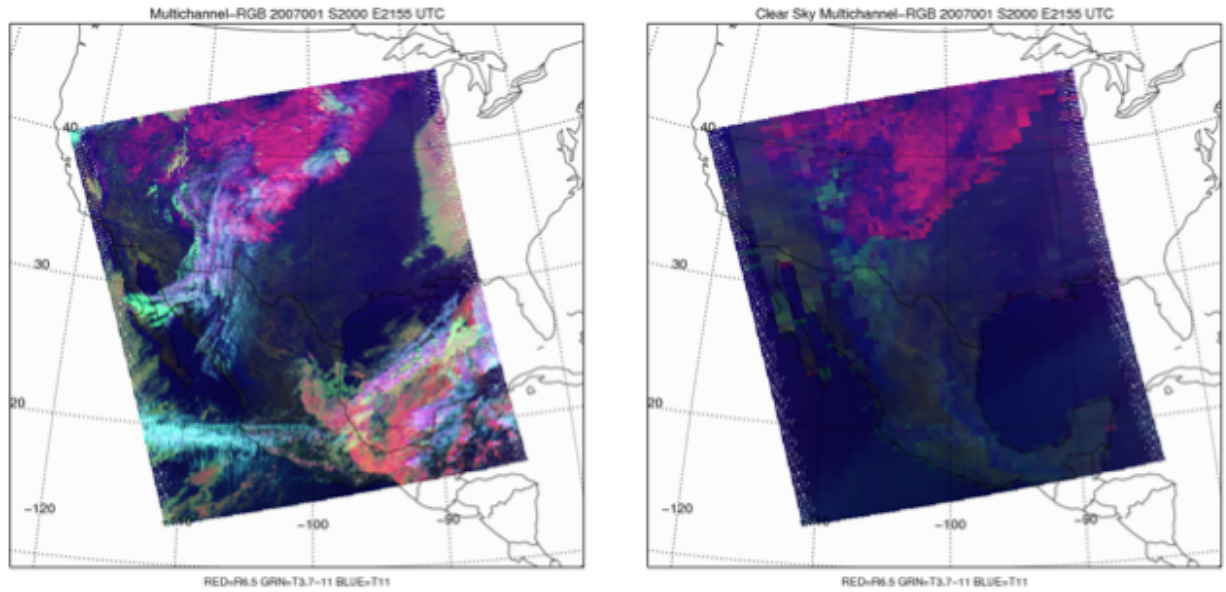

Fig. 6. Example of RGB images for a NOAA-18 AVHRR scene (2155 UTC, 1 January 2007) using VIS reflectance (red), BTD_{34} (green), and IRW BT (blue). (left) AVHRR observations and (right) simulated clear-sky scene.

unless the tile contains a significant number of clear pixels. In that case, the average reflectance is used. The albedo maps are produced for both snow-free and snow-covered conditions. Figure 5 shows an example for January 2008.

A visual quality control system was developed that converts the predicted clear-sky radiances for the VIS, IRW, and SIR channels into an RGB image that can be compared with RGB images constructed from the observed radiances in similar fashion to spot check the predicted clear-sky radiance fields. Figure 5 shows an example over southern North America during January 2007. Snow-covered areas appear in bright magenta, while water and forested areas tend to be darker blues and dry land or leafless deciduous areas are brownish-green depending on the skin temperatures. The blockiness in the simulated image results from the resolution of the temperature and snow cover fields in the input data, as well as unresolved coastlines. The speckled edges are plotting artifacts.

2.2.3 Cloud mask

The CERES Ed4 cloud mask represents a significant improvement over the Ed2 version (Minnis et al. 2008) because it uses several additional channels available on MODIS, but not on AVHRR. To better match the CERES Ed4 results, the CERES Ed2 mask, which relies primarily on the MODIS equivalents of the AVHRR channels, was adapted and refined in an attempt to make it produce results similar to those from the CERES Ed4 scene identification scheme. This took many FTE-months of iterative work using CALIPSO and interactive analyses. Figure 7 shows the mean October 2008 regional combined day and night cloud fractions from NOAA-18, Aqua MODIS from the CERES and MODIS Atmospheres Science Team Collection 5 (MAST, Menzel et al. 2008), CMSAF NOAA-18 AVHRR (Karlsson et al. 2013), ISCCP, and CALIPSO (Winker et al. 2007). The agreement is generally within 0.10 or less for most regions. The greatest differences are over Antarctica and the Arctic.

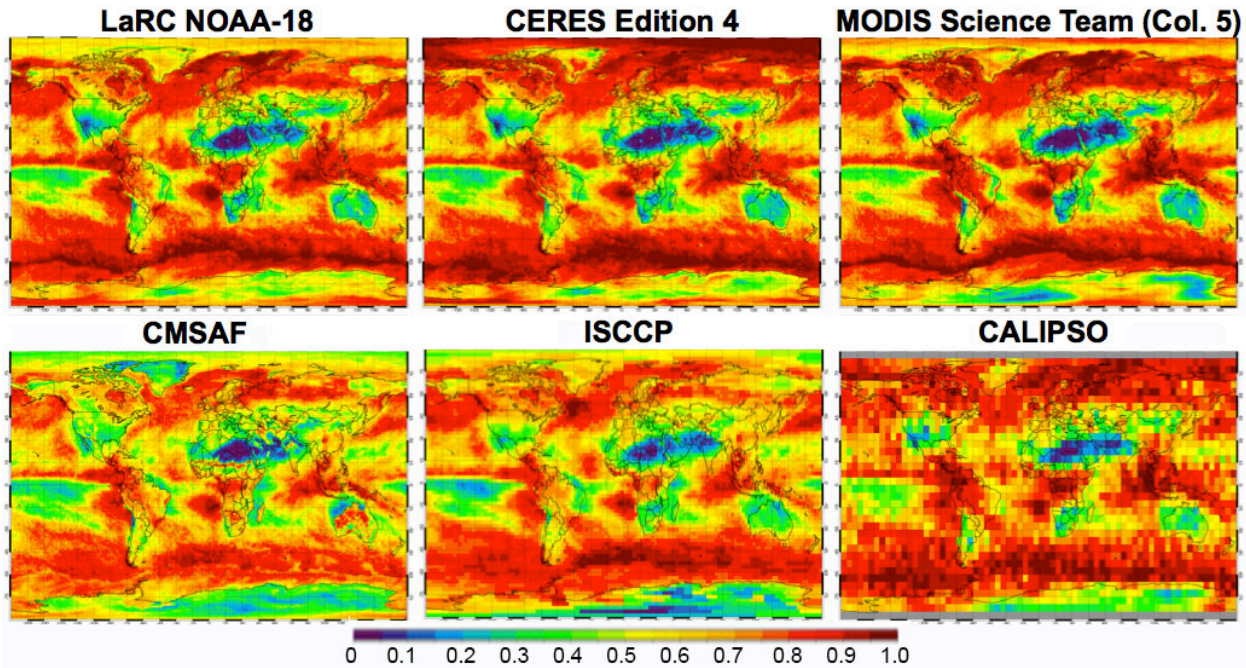

Fig. 7. Average day + night cloud fraction for October 2008 from AMCPRS NOAA-18 AVHRR, CERES Aqua MODIS, MAST Aqua MODIS C5, CMSAF NOAA-18 AVHRR, ISCCP, and CALIPSO.

The results, except for ISCCP, are separated by day and night and plotted as zonal average cloud fractions in Fig. 8. During daytime, the AMCPRS tracks the CERES CF in the northern tropics and midlatitudes, and southern midlatitudes, but exceeds CERES in the subtropics and is less than CERES in the polar regions. At night, the AMCPRS CF tracks CERES well everywhere except in the polar regions. Cloud detection during polar night is difficult with only the AVHRR channels. The greatest CF differences among the methods occur at night, when the CMSAF CF is the lowest at nearly all latitudes.

The same programs were applied to AVHRR data from NOAA-16, which had an equatorial crossing time (ECT) close to 1700 LT and viewed the same areas under much higher solar zenith angles (SZA) than NOAA-18 at 1330 LT. The results are quite comparable to those in Fig. 7,

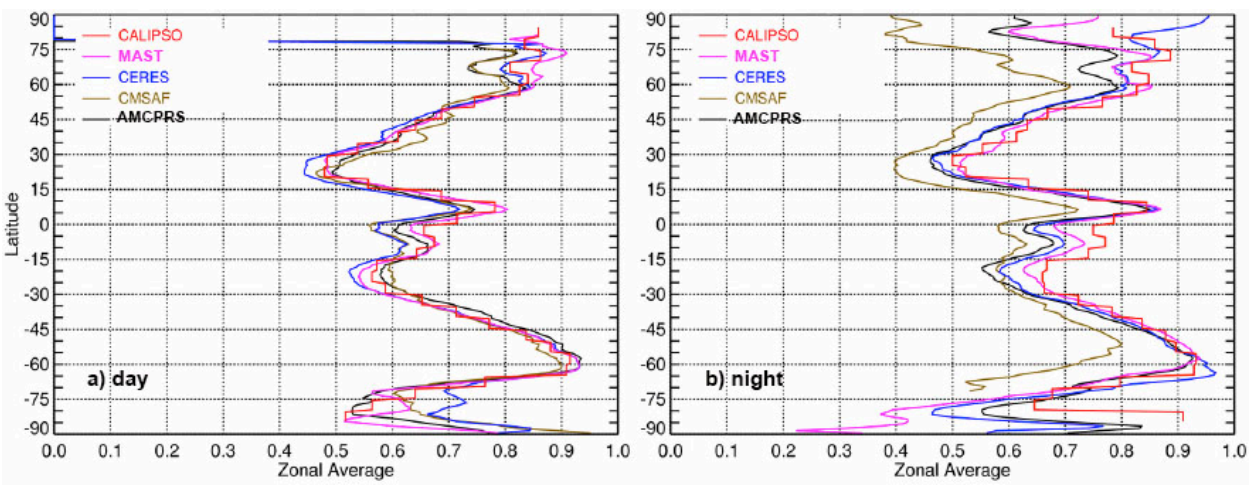

Fig. 8. Mean zonal cloud fraction for October 2008 from Aqua MODIS (MAST & CERES), NOAA-18 AVHRR (AMCPRS & CMSAF), and CALIPSO.

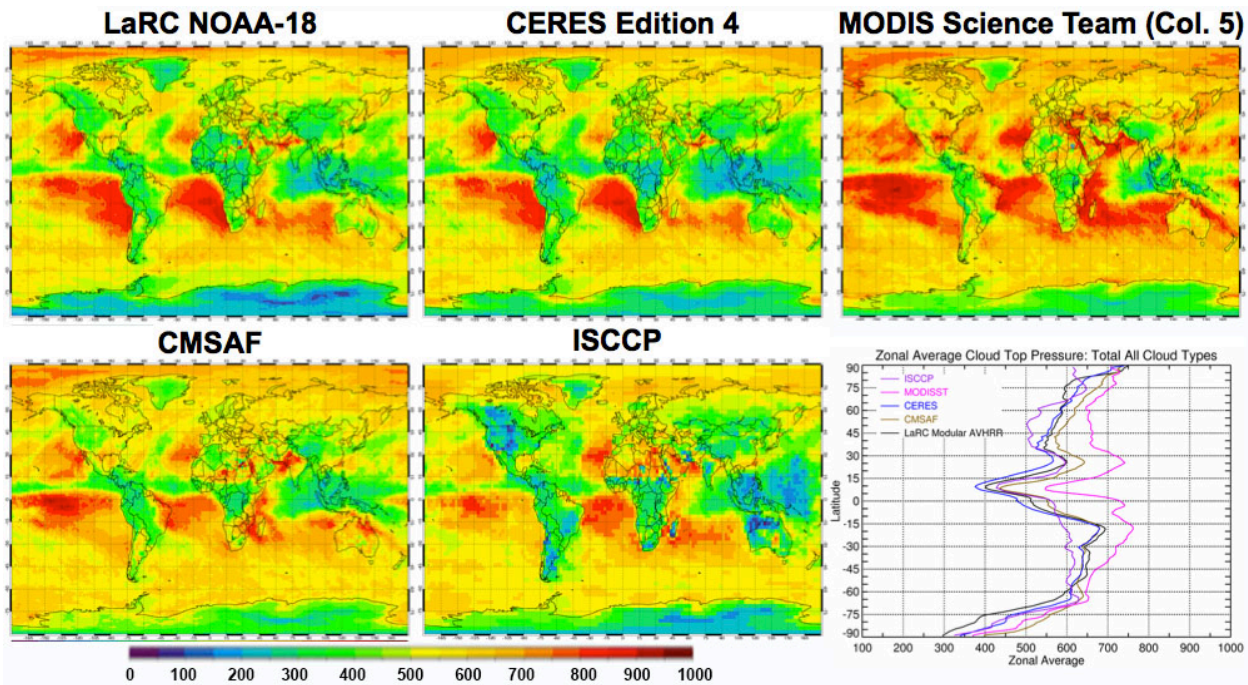

Fig. 9. Mean October 2008 cloud top pressure from Aqua MODIS (MAST & CERES), NOAA-18 AVHRR (AMCPRS & CMSAF), and ISCCP.

except that the cloud cover in the polar regions is severely overestimated. These results and other analyses using NOAA-15 in a near-terminator orbit indicate that only data from SZA less than a particular value should be considered useful for daytime analysis. Further study of the exact threshold and possible ways for overcoming the extreme viewing conditions are being examined. For example, the NOAA-15 near-terminator orbit not only places most of the areas in a high ZA conditions, but the lowest SZA regions are observed in extreme sunglint. Such problems need to be resolved before the data can be analyzed and archived. Thus, for the time being, only nighttime data and data from orbits having an ECT within 4-5 hours of local noon will be considered as climate worthy.

Matched CALIPSO and AMCPRS pixels during October 2008 were used to evaluate the cloud mask. From a total of ~167,000 matches, it was found that for daytime (SZA $\leq$ 82°), the fraction correct (FC) was 86.4% with a slight (1.8%) overestimate of cloud cover. At night, (SZA $\geq$ 88.5°), FC = 82.7% with a 4% underestimate using 177,000 pixels. In near-terminator conditions (82° < SZA < 88.5°), FC = 0.801 with an underestimate of 8.5% for only 16,300 pixels. It should be noted that CALIPSO is more sensitive at night and detects more clouds. These FC statistics are slightly worse than those for CERES. Such a decrease in accuracy is expected for several reasons. Fewer channels are available to the AMCPRS mask, the data are lower in resolution and are sampled so that the matching is less accurate. The slight daytime overestimate may be due to the higher viewing zenith angles (VZA) of the AVHRR. For the CERES and CALIPSO comparisons, both instruments having near-nadir viewing, while the AVHRR data are taken at all VZA < 70°. Cloud detection increases with VZA due to the vertical dimension of clouds.

2.2.4 Cloud top pressure and height

Once identified, the clouds are analyzed to produce cloud effective temperature, pressure, and height: CET, CEP, and CEH, respectively. The cloud optical depth and particle effective

Table 2. AMCPRS – CALIPSO CTH in km for single-layer clouds, October 2008.

	Mean diff (day)	STD DEV (day)	Mean diff (nite)	STD DEV (nite)
Thin ice	-1.50	3.25	-0.98	3.39
Thick ice	-0.78	1.42	-0.43	1.49
Thin water	-0.02	1.03	0.22	0.84
Thick water	-0.01	0.75	0.45	0.85

radius, COD and CER, respectively, are retrieved simultaneously. The cloud top temperature, pressure, and height: CTT, CTP, and CTH, respectively, are then determined using an empirical approach. The October 2008 results for NOAA-18 AVHRR are compared to those from other methods in Fig. 9. There are areas of generally good agreement, but in many regions one or more of the retrievals differ, particularly over the marine stratus regions. The zonal averages are close for CERES, CMSAF, and AMCPRS, while the MAST pressures are much greater overall and the ISCCP pressures in the subtropics and lower midlatitudes are less than all of the others.

Comparisons of AMCPRS and CALIPSO single-layer CTHs (Table 2) show that the liquid cloud CTH are unbiased during the daytime, but are too high by ~0.3 km at night. The ice CTH means are less than the CALIPSO CTHs by 0.4 to 1.5 km depending on time of day and COD. Thick clouds are defined as those having COD > 6. A total of 26,750 pixels were used for the daytime analysis, while the nighttime comparisons are from 19,500 pixels. The uncertainties in the thin ice CTH are more than twice those for thick ice clouds. The nighttime bias in the liquid CTH is unexpected, because it was not seen in similar comparisons with CERES and requires further study.

2.2.5 Cloud phase, optical depth, and effective radius

The cloud phase for single-layer clouds was examined by comparing with that from matched CALIPSO retrievals. For ~52,300 daytime pixels, FC = 92.2% with a 0.5% bias toward liquid clouds. At night, the 54,000 matched pixels yielded FC = 90.4% with a 1% bias for liquid clouds. FC = 77.7% for the near-terminator pixels and the bias is 19.1% for ice clouds. These results suggest further work is needed on the near-terminator cases. Such work will be critically important for orbits late in the lifetimes of many of the AVHRRs and for those that began with a 0730 ECT orbit.

The CODs from 2008 were averaged linearly and compared with those from CERES, MAST, and CMSAF. The results show similar patterns, except in the polar regions. The MAST results tend to be much greater because the MAST C5 analysis systematically removed low optical depth clouds along cloud edges to ensure that only the most reliable values were retrieved (see Platnick et al. 2013; Minnis et al. 2011b; Stubenrauch et al. 2013). This difference is most clearly seen in the zonal averages. The AMCPRS means are less than those from CERES, in general, and sometimes less (northern hemisphere) or greater (southern hemisphere) than those from CMSAF. For nonpolar areas, the CERES and AMCPRS ice COD means agree quite well, but the underestimate is systematic at all latitudes

The lower CODs from the AVHRR retrievals relative to CERES can be due to several factors. One is resolution. We examined the resolution effect by retrieving cloud properties from 1-km MODIS data over the central USA at the native resolution and at 2 and 4-km resolutions. The reduced resolutions were obtained by averaging the MODIS 1-km radiances for sets 4 and 16 pixels. The results showed that there was negligible impact on water and ice cloud fractions, but mean CTP increased by 4 and 9 hPa for the 2 and 4-km resolutions, respectively. The corresponding average liquid CODs decreased 6 and 13%, but the difference in ice COD was

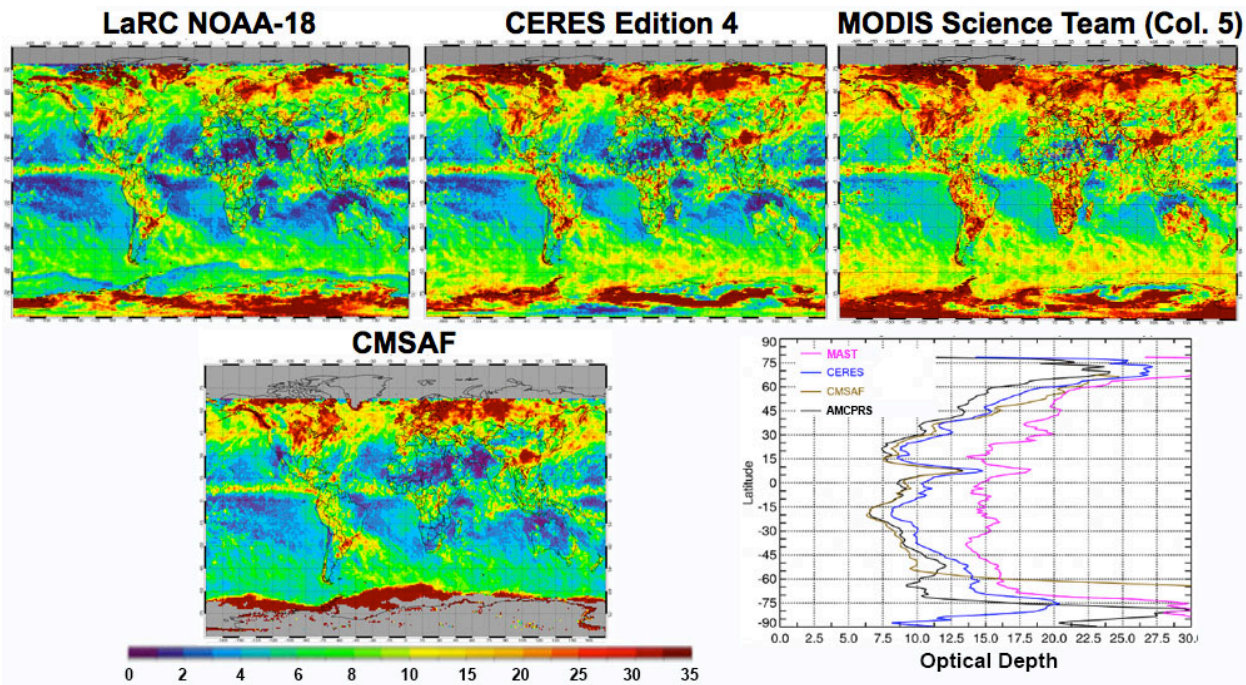

Fig. 10. Mean October 2008 cloud optical depth from Aqua MODIS (MAST & CERES) and NOAA-18 AVHRR (AMCPRS & CMSAF).

negligible. Since the AVHRR GAC data represent an average of 4 1-km pixels, resolution differences could explain about half of the mean COD difference, which is ~10% for 60°N – 60°S.

In addition to differences in the detected clouds, which could have different CODs on average, calibration differences could also be responsible for the COD discrepancies with CERES. For the solar channels, the third version of AVHRR uses a dual-gain calibration that has a breakpoint around 500 counts. This calibration is not taken into account when the GAC averaging is performed. Thus, the average counts near the breakpoint can be biased in terms of reflectance. The calibration of AVHRR to the MODIS reference uses GAC data with an effective single gain approach that includes this breakpoint artifact. It could influence the calibration by introducing a shift in the derived gain. This effect is being investigated further. Retrieving accurate values of COD is critical for computing the radiation budget from these data. Recent unpublished studies indicate that when the CERES CODs are used in a radiative transfer model, the TOA broadband shortwave reflected radiative fluxes agree to within ± 1 Wm^{-2}. The relative bias in the current AMCPRS results would not yield the same type of accuracy. Thus, obtaining consistency with CERES, at least for the nonpolar regions, requires understanding and mitigating the COD differences.

The mean zonal values for CER are shown in Fig. 11 for AMCPRS, CERES, and MAST for data taken during October 2008. The CERES and AMCRPRS ice CER values (Fig. 11a) are in good agreement between 50°N and 50°S. In the polar regions, particularly around Antarctica, the values diverge. The disagreement over the polar regions is not unexpected given the large differences in COD values arising from the different channels used to retrieve COD. Both the CERES and AMCPRS means increase with latitude, unlike the MAST and CERES Ed2 (Minnis et al. 2011b, not shown). This latitudinal dependence appears to be the result of temperature dependence of the particle size as plotted in Fig. 12 for the CERES data.

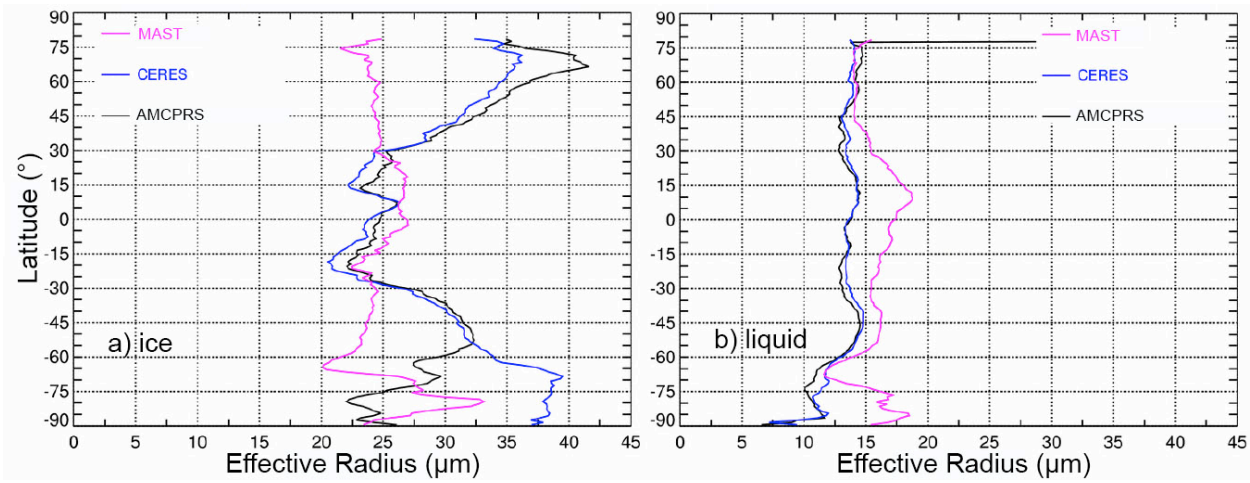

Fig. 11. Mean zonal cloud effective radius, October 2008.

The CERES and AMCPRS liquid cloud CER means (Fig. 11b) are very close, differing by less than ±0.5 μm at most latitudes. Both are smaller than their MAST counterparts, which are based on retrievals using the 2.1-μm channel instead of the 3.8-μm channel. Similar differences have been noted previously (e.g., Minnis et al. 2011b).

2.2.6 Skin temperature

The surface skin temperature T_{skin} for clear pixels is being retrieved using a single-channel (10.8-μm) approach (Scarino et al. 2013). No corrections are applied to account for viewing and illumination angle dependencies. Figure 13 shows an example of T_{skin} retrieved over the ARM SGP in central Oklahoma and compared with the temperature from the down-view infrared thermometer. The AVHRR retrieval is, on average, 0.7 K less than its surface-based counterpart with and RMS difference of 2.7 K. Some of the bias is due to shadowing during the day that causes the satellite to sometimes see colder portions of the scene than the IRT. Similar or better results were found over other sites and compared to the MODIS Land Team's retrievals (Scarino et al. 2013). Application of a VZA-dependent surface emissivity could reduce the RMS differences.

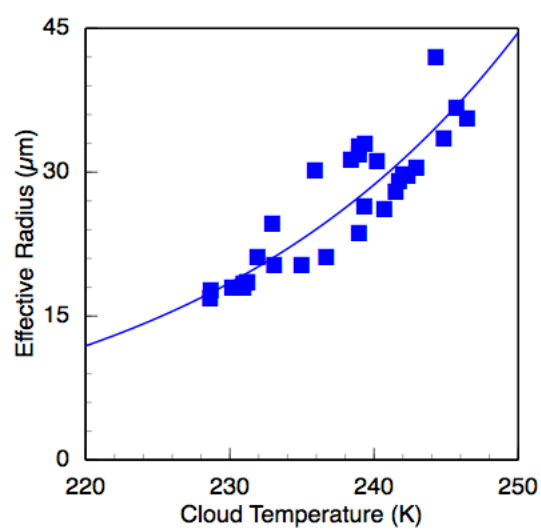

Fig. 12. Zonal mean CERES ice particle effective radius as a function of cloud effective temperature.

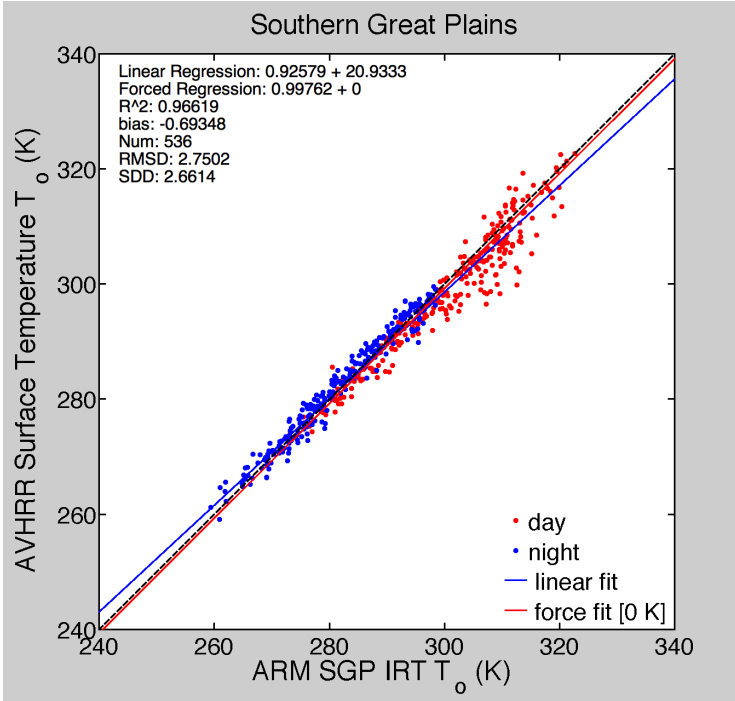

Fig. 13. AVHRR Land Surface Temperature compared to matched ARM SGP IRT temperatures, January-December 2008.

3.0 Tasks Ahead

The delivery of the first datasets was delayed by the some of the problems noted above and others that have not been yet been discussed. They include the adjustment of the algorithm to retrieve more accurate cloud properties over snow, in sunglint, and in extreme SZA conditions. The complement of channels available from MODIS enabled us to develop reasonable approaches to those problems. The absence of those channels on AVHRR has diminished our capability to address those troublesome conditions. Thus, a considerable, iterative effort has been devoted to resolving the discrepancies in those conditions with ambiguous success. Additionally, no IR calibrations for the old AVHRRs have become available. To ensure the best quality cloud CDR, we have revised the strategy to analyze the data in the following way.

3.1 Resolve outstanding calibration issues

The dual-gain slope problem noted above must be solved before delivering the first datasets. This is critical because of its effect on COD. We expect that this issue can be addressed using the original 1-km AVHRR data. Exceptions for the reduced dynamic infrared range of some older AVHRRs must be developed. For example, the NOAA-9 AVHRR IRW channel maximum temperature is ~325 K compared to 340 K for NOAA-18. Differences among the ranges in the 3.7-µm channels must also be taken into account (Fig. 3).

3.2 Polar regions

The approach to retrieving cloud properties over snow with the limited AVHRR channels has been to use the VIS channel for thick clouds and the nighttime algorithm during the day for thin clouds. This combination explains the smaller values of COD in the AMCPRS means in Fig. 10. The remaining obstacle is deciding when to apply one or the other algorithm. Also, the nighttime

cloud mask over the polar regions needs to be refined because of the extreme noise in the SIR channel at the low end of its range.

3.3 Revised strategy

The data delivery will follow the strategy outlined below.

First, the post N-14 AVHRR datasets with daytime 3.7-µm channels will be processed for nighttime and daytime for all months having an ECT within 4.5 – 5.0 hours of local noon to minimize the currently overwhelming uncertainties in the retrievals for near-terminator orbits. These data will be delivered before June 2014.

Next, the pre-N14 AVHRR datasets having all 5 channels will be processed using the same ECT constraints. These will be followed by the AVHRR datasets having 4 channels (no 12-µm channel) back to TIROS-N. Next, the AVHRR/3 sensors having only 1.6-µm data during the day will be analyzed. Finally, all-near-terminator orbit data will processed using the best algorithm available at the time.

3.4 Documentation

The Implementation plans have been delivered and the FCDR C-ATBD is nearly complete. The FCDR C-ATBD will be delivered before May 2014, while the codes for both the TCDR and FCDR will be delivered in June 2014.

References

Doelling, D. R., R. Bhatt, D. Morstad, and B. Scarino, 2011a: Algorithm Theoretical Basis Document (ATBD) for ray-matching technique of calibrating GEO sensors with Aqua-MODIS for GSICS. (https://gsics.nesdis.noaa.gov/pub/Development/AtbdCentral/GSICS_ATBD_RayMatch_NASA_2011_09.pdf)

Doelling, D. R., R. Bhatt, D. Morstad, and B. Scarino, 2011b: Algorithm Theoretical Basis Document (ATBD) for Deep Convective Cloud (DCC) technique of calibrating GEO sensors with Aqua-MODIS for GSICS. (https://gsics.nesdis.noaa.gov/pub/Development/AtbdCentral/GSICS_ATBD_DCC_NASA_2011_09.pdf)

Heidinger, A. K., W. C. Straka III, C. C. Molling, J. T. Sullivan, and X. Wu, 2010: Deriving an inter-sensor consistent calibration for the AVHRR solar reflectance data record. *Intl. J. Remote Sens.*, 31, 6493-6517.

Karlsson, K.-G., Riihelä, A., Müller, R., Meirink, J. F., Sedlar, J., Stengel, M., Lockhoff, M., Trentmann, J., Kaspar, F., Hollmann, R., and Wolters, E., 2013: CLARA-A1: the CM SAF cloud, albedo and radiation dataset from 28 yr of global AVHRR data. *Atmos. Chem. Phys.*, **13**, 5351-5367, doi:10.5194/acp-13-5351-2013.

Khlopenkov K. V. and A. P. Trishchenko, 2010: Achieving subpixel georeferencing accuracy in the Canadian AVHRR processing system. *IEEE Trans. Geosci. Remote Sens.*, **48**, 2150–2161.

Menzel, P., R. A. Frey, H. Zhang, D. P. Wylie, C. C. Moeller, R. E. Holz, B. Maddux, et al., 2008: MODIS global cloud-top pressure and amount estimation: Algorithm description and results. *J. Appl. Meteorol. Climatol.*, 47, 1175-1198.

Minnis, P., D. R. Doelling, L. Nguyen, W. F. Miller, and V. Chakrapani, 2008: Assessment of the visible channel calibrations of the TRMM VIRS and MODIS on *Aqua* and *Terra*. *J. Atmos. Oceanic Technol.*, **25**, 385-400.

Minnis, P., S. Sun-Mack, Q. Z. Trepte, F.-L. Chang, P. W. Heck, Y. Chen, Y. Yi, R. F. Arduini, K. Ayers, K. Bedka, S. Bedka, R. Brown, S. Gibson, E. Heckert, G. Hong, Z. Jin, R. Palikonda, R. Smith, W. L. Smith, Jr., D. A. Spangenberg, P. Yang, C. R. Yost, and Y. Xie, 2010a: CERES Edition 3 cloud retrievals. *AMS 13th Conf. Atmos. Rad.*, Portland, OR, June 27 – July 2, 5.4.

Platnick, S., M. D. King, S. A. Ackerman, W. P. Menzel, B. A. Baum, J. C. Riedl, and R. A. Frey, 2003: The MODIS cloud products: Algorithms and examples from Terra. *IEEE Trans. Geosci. Remote Sens.*, **41**, 459-473.

Rossow, W. B. and R. A. Schiffer, 1999, Advances in understanding clouds from ISCCP. *Bull. Amer. Meteorol. Soc.*, **80**, 2261-2287.

Simpson, J. J. and S. R. Yhann (1994), Reduction of noise in AVHRR channel 3 data with minimum distortion, *IEEE Trans. Geosci. Remote Sens.*, 32, 315-328.

Winker. D. M., W. Hunt, and M. J. McGill (2007), Initial performance assessment of CALIOP, *Geophys., Res. Lett.*, **34**, L19803, doi:10.1029/2007GL030135.

Publications and presentations to date (some also referenced)

Peer-reviewed Papers and ATBDs

Bhatt, R., D. R. Doelling, D. Morstad, B. R. Scarino, and A. Gopalan, 2013: Desert-based absolute calibration of successive visible sensors using a daily exoatmospheric radiance model. *IEEE Trans. Geosci. Remote Sens.,* doi:10.1109/TGRS.2013.2274594.

Chander, G., N. Mishra, D. L. Helder, D. B. Aaron, A. Angal, T. Choi, X. Xiang, and D. R. Doelling, 2013: Applications of spectral band adjustment factors (SBAF) for cross-calibration. *IEEE Trans. Geosci. Remote Sens.*, **51**, 1147-1159, doi:10.1109/TGRS.2012.2228007.

Doelling, D. R., C. Lukashin, P. Minnis, B. Scarino, and D. Morstad, 2012: Spectral reflectance corrections for satellite intercalibrations using SCIAMACHY data. *Geosci. Remote Sens. Lett.*, **9**, 119-123, doi: 10.1109/LGRS.2011.2161751.

Doelling, D. R., B. R. Scarino, D. Morstad, A. Gopalan, R. Bhatt, C. Lukashin, and P. Minnis, 2013a: The calibration of visible imagers using operational hyperspectral SCIAMACHY radiances. *IEEE Trans. Geosci. Remote Sens.*, **51**, 1245-1254, doi:10.1109/TGRS.2012.2227760.

Doelling, D. R. and P. Minnis (2013), Calibration of historical and future AVHRR and GOES visible and near-infrared sensors Climate Algorithm Theoretical Basis Document (C-ATBD). *NOAA C-ATBD DSR-XXX*, under revision.

Doelling, D. R., D. Morstad, B. R. Scarino, R. Bhatt, and A. Gopalan, C, 2013b: The characterization of deep convective clouds as an invariant calibration target and as a visible calibration technique. *IEEE Trans. Geosci. Remote Sens.*, **51**, 1147-1159, doi:10.1109/TGRS.2012.2225066.

Goldberg, M., G. Ohring, J. Butler, C. Cao, R. Datla, D. Doelling, V. Gärtner, T. Hewison, B. Iacovazzi, D. Kim, T. Kurino, J. Lafeuille, P. Minnis, D. Renaut, J. Schmetz, D. Tobin, L. Wang, F. Weng, X. Wu, F. Yu, P. Zhang, and T. Zhu, 2011: The Global Space-based Inter-Calibration System (GSICS). *Bull. Am. Meteorol. Soc.*, **92** (4), 467-475.

Minnis, P. and K. M. Bedka (2014), A consistent long-term cloud and clear-sky radiation property dataset from the Advanced Very High Resolution Radiometer (AVHRR), Climate

Algorithm Theoretical Basis Document (C-ATBD). *NOAA C-ATBD DSR-XXX*, in preparation.

Scarino, B., P. Minnis, R. Palikonda, R. Riechle, D. Morstad, C. Yost, B. Shan, and Q. Liu, 2013: Deriving surface skin temperature for NWP applications using global geostationary satellite data. *Remote Sens.*, **5**, 342-366, doi:10.3390/rs5010342.

Shrestha, A. K., S. Kato, T. Wong, D. A. Rutan, W. F. Miller, F. G. Rose, G. L. Smith, K. M. Bedka, P. Minnis, and J. R. Fernandez-Sanginez, 2014: Unfiltering Earth Radiation Budget Experiment (ERBE) scanner radiances using the CERES algorithm and its evaluation with nonscanner observations. In press, *J. Atmos. Oceanic Tech.*

Wu, A., X. Xiong, D. R. Doelling, D. Morstad, A. Angal, and R. Bhatt, 2013: Characterization of Terra and Aqua MODIS, VIS, NIR, and SWIR spectral bands' calibration stability. *IEEE Trans. Geosci. Remote Sens.*, **51**, 4430-4438, doi:10.1109/TGRS.2012.2226588.

Conference Proceedings

Bhatt, R., D. R. Doelling, B. R. Scarino, A. Gopalan, and C. O. Haney, 2013b: An initial assessment of the VIIRS onboard calibration using DCC and desert referenced to the Aqua-MODIS calibration. *Proc. of SPIE Vol. 8866,* 88660K.

Bhatt, R., D. R. Doelling, and B. R. Scarino, 2012: Desert based absolute calibration of visible sensors. *IEEE Geosci. Remote Sens. Symp. (IGARSS)*, 7015-7018. doi: 10.1109/IGARSS.2012.6351956.

Scarino, B., D. R. Doelling, D. L. Morstad, R. Bhatt, C. Lukashin, and P. Minnis, 2012: Using SCHIAMACHY to improve corrections for spectral and differences when transferring calibration between visible sensors. *Proc. SPIE Conf. 8510, Earth Observing Systems XVII*, San Diego, CA, 13-16 August, 8150-25.

Conference Presentations

Bedka, K., P. Minnis, D. Doelling, R. Palikonda, Q. Trepte, P. Heck, K. Khlopenkov, and B. Scarino, 2012: Efforts toward a 30-year AVHRR cloud property climate data record. *AMS 18th Conf. Satellite Meteor., Oceanog., and Climatol.*, New Orleans, LA, 22 -26 January, P475.

Bedka, K., P. Minnis, D. Doelling, R. Palikonda, Q. Trepte, P. Heck, B. Scarino, S. Bedka, C. Yost, R. Bhatt, A. Gopalan, K. Khlopenkov, and G. Hong, 2013: Extending the CERES cloud climate record using MODIS and AVHRR data. *CERES Spring Sci. Team Mtg.*, Newport News, VA, 7-9 May.

Bedka, K. R. Palikonda, and P. Minnis, 2012: A CERES-consistent cloud climate record from AVHRR data. *4th WCRP Intl. Conf. Reanalyses*, Silver Spring, MD, 7-11 May.

Bhatt, R., D. R. Doelling, D. Morstad, B. R. Scarino, and A. Gopalan, The vicarious calibration of geosynchronous and polar-orbiting visible sensors using desert BRDF models based on the TRMM VIRS imager. *AMS 9th Ann. Symp. Future Oper. Environ. Sat. Sys.*, Austin, TX, Jan. 5-10, 705.

Bhatt, R., D. Doelling, B. Scarino, A. Gopalan, and C. Haney, 2013: Desert-based calibration of geostationary visible sensors using a daily exoatmospheric radiances model (DERM). *GSICS Ann. Mtg.*, Williamsburg, VA, Mar. 4-8.

Doelling, D., B. Scarino, D. Morstad, R. Bhatt, and A. Gopalan, 2012: Using hyper-spectral SCIAMACHY radiances to uniformly calibrate contemporary geostationary visible imagers. *CALCON 2013*, Logan, UT, Aug. 27- 30.

Doelling, D. D. Morstad, B. Scarino, R. Bhatt, and A. Gopalan, 2013: On the path towards reference sensor calibration transfer using DCC invariant targets. *GSICS Ann. Mtg.*, Williamsburg, VA, Mar. 4-8.

Khlopenkov, K. and P. Minnis, 2011: Analysis and improvement of geo-referencing accuracy in long term global AVHRR data. *AGU Fall Mtg 2011*, 5-9 December, San Francisco, CA, IN21A-1413.

Minnis, P., K. Bedka, D. R. Doelling, Q. Trepte, R. Palikonda, K. Khlopenkov, B. R. Scarino, and D. Morstad, 2011: Calibration of historical and future AVHRR and GOES visible and near-infrared sensors and the development of a consistent long-term cloud and clear-sky radiation property dataset. *NOAA CDR Annual Team Mtg.*, Asheville, NC, August 2-4.

Minnis, P., K. Bedka, D. R. Doelling, A. Gopalan, R. Palikonda, K. Khlopenkov, B. R. Scarino, Q. Trepte, and D. Morstad, 2012: Calibration of historical and future AVHRR and GOES visible and near-infrared sensors and the development of a consistent long-term cloud and clear-sky radiation property dataset. *NOAA CDR Annual Team Mtg.*, Asheville, NC, July 31 - August 2.

Minnis, P., K. Bedka, D. R. Doelling, R. Palikonda, S. Bedka, R. Bhatt, T. Chee, A. Gopalan, C. Haney, G. Hong, K. Khlopenkov, B. R. Scarino, Q. Trepte, and C. Yost, 2013: Calibration of historical and future AVHRR and GOES visible and near-infrared sensors and the development of a consistent long-term cloud and clear-sky radiation property dataset. *NOAA CDR Annual Team Mtg.*, Asheville, NC, July 30 - August 1.

Minnis, P., K. Bedka, R. Palikonda, Q. Trepte, P. Heck, B. Scarino, S. Bedka, C. Yost, R. Bhatt, A. Gopalan, K. Khlopenkov, G. Hong, and D. Doelling, 2013: A CERES-consistent cloud property and surface temperature climate data record using AVHRR data. *NOAA 2013 Satellite Conf. Direct Readout, GOES/POES, and GOES-R/JPSS Users*, College Park, MD, April 8-12.

Minnis, P., D. R. Doelling, K. T. Bedka, R. Palikonda, Q. Z. Trepte, S. Bedka, B. Scarino, D. Morstad, and P. W. Heck, 2011: A CERES-like cloud property data record from AVHRR data. *2011 EUMETSAT Meteorol. Sat. Conf., Oslo, Norway, Sept. 5 – 9.*

Minnis, P., R. Palikonda, F.-L. Chang, W. L. Smith, Jr., J. K. Ayers, K. Bedka, R. Boeke, Y. Chen, P. Heck, M. M. Khaiyer, D. A. Spangenberg, S. Sun-Mack, Q. Trepte, Y. Yi, and C. Yost, 2011: Updated NASA Langley cloud property retrievals. *3rd EUMETSAT Cloud Property Retrieval Workshop, CREW-3*, 15-18 November, Madison, WI.

Minnis, P. S. Sun-Mack, R. Palikonda, Q. Z. Trepte, Y. Chen, R. F. Arduini, X. Dong, B. Xi, and K. Giannechi, 2011: Retrieving cloud optical properties over snow and ice covered surfaces. *2011 EUMETSAT Meteorol. Sat. Conf., Oslo, Norway, Sept. 5 – 9.*

Morstad, D., R. Bhatt, B. Scarino, A. Gopalan, and D. Doelling, 2012: Characterization of deep convective clouds as absolute calibration targets for visible sensors. *CALCON 2013*, Logan, UT, Aug. 27- 30.

Rienecker, M. M., M. J. Suarez, R. Gelaro, R. Todling, J. Bacmeister, E. Liu, M. G. Bosilovich, S. D. Schubert, L. Takacs, G.-K. Kim, S. Bloom, J. Chen, D. Collins, A. Conaty, and A. da Silva, et al. (2011). MERRA - NASA's Modern-Era Retrospective Analysis for Research and Applications. *J. Climate*, 24, 3624-3648, doi:10.1175/JCLI-D-11-00015.1.

Scarino, B., D. R. Doelling, D. Morstad, P. Minnis, and C. Lukashin, 2012: The calibration of LEO and GEO satellite imager radiances using hyper-spectral data from SCIAMACHY. *AMS 8th Ann. Symp. Future Oper. Environ. Satellite Sys.*, New Orleans, LA, 22 -26 January, P494.

Scarino, B., D. R. Doelling, P. Minnis, R. Bhatt, A. Gopalan, and C. Lukashin, 2013: Spectral band adjustment factors in the shortwave. *GSICS Ann. Mtg.*, Williamsburg, VA, Mar. 4-8.

Scarino, B., P. Minnis, R. Palikonda, P. H. Heck, and K. Bedka, 2013: Land and ocean surface skin temperature from geostationary and low Earth orbit satellite observations. *AGU Fall Mtg 2013*, 9-13 December, San Francisco, CA, GC41A-0985.

Shrestha, A. K., S. Kato, K. M. Bedka, P. Minnis, W. F. Miller, and T. E. Caldwell, 2011: Improvement of ERBE-derived TOA irradiance with AVHRR data and Aqua CERES angular distribution models. *AGU Fall Mtg 2011*, 5-9 December, San Francisco, CA, U41B-0010.

Trepte, Q., P. Minnis, R. Palikonda, K. Bedka, and S. Sun-Mack, 2011: Comparison of cloud detection using the CERES Ed4 and LaRC AVHRR cloud masks and CALIPSO Version 3 Vertical Feature Mask. *AGU Fall Mtg 2011*, 5-9 December, San Francisco, CA, A13B-0234.